Controlled molecular self-assembly of complex three-dimensional structures in soft materials

Changjin Huang[a], David Quinn[b], Subra Suresh[c,1], and K. Jimmy Hsia[a,b,1]

[a]Department of Biomedical Engineering, Carnegie Mellon University, Pittsburgh, PA 15213; [b]Department of Mechanical Engineering, Carnegie Mellon University, Pittsburgh, PA 15213; and [c]Nanyang Technological University, Singapore 639798, Republic of Singapore

Contributed by Subra Suresh, November 21, 2017 (sent for review October 13, 2017; reviewed by Guruswami Ravichandran and Zhigang Suo)

Many applications in tissue engineering, flexible electronics, and soft robotics call for approaches that are capable of producing complex 3D architectures in soft materials. Here we present a method using molecular self-assembly to generate hydrogel-based 3D architectures that resembles the appealing features of the bottom-up process in morphogenesis of living tissues. Our strategy effectively utilizes the three essential components dictating living tissue morphogenesis to produce complex 3D architectures: modulation of local chemistry, material transport, and mechanics, which can be engineered by controlling the local distribution of polymerization inhibitor (i.e., oxygen), diffusion of monomers/cross-linkers through the porous structures of cross-linked polymer network, and mechanical constraints, respectively. We show that oxygen plays a role in hydrogel polymerization which is mechanistically similar to the role of growth factors in tissue growth, and the continued growth of hydrogel enabled by diffusion of monomers/cross-linkers into the porous hydrogel similar to the mechanisms of tissue growth enabled by material transport. The capability and versatility of our strategy are demonstrated through biomimetics of tissue morphogenesis for both plants and animals, and its application to generate other complex 3D architectures. Our technique opens avenues to studying many growth phenomena found in nature and generating complex 3D structures to benefit diverse applications.

soft matter | morphogenesis | polymerization | 3D structures

Living tissues of plants or animals form complex three-dimensional (3D) shapes and patterns to achieve their functions. For example, directional bending of plant stems in response to changes in the directions of light and gravity enables the leaves to improve their photosynthesis efficiency (1). Similarly, the formation of individual villi in human gut facilitates better absorption of nutrients (2). Tissue growth is a result of individual cell growth and/or cell proliferation during which new biomass is synthesized by consuming nutrients that are taken up locally in animals or plants and transported to other regions of their structures via vascular systems (3). In contrast to other growth mechanisms such as solidification of metals where growth is accomplished by adding newly solidified materials onto the surface (4–7), the continuous insertion of new biomass into existing structures makes living tissue growth a unique phenomenon. Furthermore, as the rate of tissue growth is dictated by the presence of growth factors, differential spatial growth in living tissues is possible with nonuniform distribution of growth factors enabled by intercellular transport (8, 9). A direct consequence of the differential spatial growth is the emergence of internal mechanical residual stress, which influences tissue morphogenesis through the following two aspects. On one hand, the growth-induced residual stress may modulate biochemical signaling pathways and stabilize the regional distribution of growth factors, enabling further increase in the stress level (10, 11). On the other hand, as the accumulated residual stress reaches a critical value, it may facilitate tissue morphogenesis by, e.g., mechanically buckling the tissue (12–15).

Differential growth of living tissues has been replicated in vitro primarily by the differential swelling of hydrogels (15–19). Engineered heterogeneity by recourse to such approaches as spatially varying the degree of cross-linking (17, 20, 21), adopting a multilayer design (18, 19, 22), or attaching the hydrogel to a rigid surface so as to impose a mechanical boundary constraint (23), has often been introduced to achieve stable differential swelling. Three-dimensional printing of layered hydrogel with stiff cellulose fibrils aligned in the printing direction engenders controlled swelling that is shown to mimic the evolution of complex 3D architectures found in nature (24). Despite their ability to generate 3D geometries, existing methods to produce complex shapes in soft materials differ fundamentally from the processes underlying tissue growth in the following distinct ways: (*i*) living tissues grow by adding new cells into existing cell aggregates, whereas no further polymerization is involved during controlled swelling of hydrogel; and (*ii*) the formation and swelling of hydrogels are two sequential processes in engineered systems, whereas in living systems, tissue growth and shape formation occur as a single, integrated process. In other words, existing methods to engineer complex 3D shapes through controlled swelling of hydrogels constitute a top-down approach; morphogenesis of living tissues, in contrast, is a bottom-up approach.

Here, we report a bottom-up approach to generating complex 3D hydrogel structures. The technique involves polymerization of monomers into polyacrylamide (PA) hydrogel. PA hydrogel has been commonly used as a scaffold biomaterial for tissue engineering owing to its appealing similarities to living tissues

Significance

We demonstrate a unique growth mode to form complex 3D shapes in hydrogels by invoking the bottom-up approach analogous to cell enlargement and proliferation found in living animal tissues and plants. For this purpose, we control the oxygen concentration to modulate polymerization of monomers in porous hydrogel, wherein postgelation networks continue to expand—a process similar to the growth of living tissues in nature. The applicability of this experimental technique to a variety of situations in biology is demonstrated with several examples of the formation of complex 3D architectures through successful biomimetics of tissue morphogenesis in both animals and plants. These results offer possibilities for a diverse set of applications in tissue engineering, soft robotics, and flexible electronics.

Author contributions: S.S. and K.J.H. designed research; C.H. performed research; C.H., D.Q., S.S., and K.J.H. analyzed data; and C.H., D.Q., S.S., and K.J.H. wrote the paper.

Reviewers: G.R., California Institute of Technology; and Z.S., Harvard University.

Conflict of interest statement: The Sponsor declares a conflict of interest. S.S. has filed for invention disclosure based on the work presented in this paper. The authors declare a conflict of interest. C.H., S.S., and K.J.H. have filed for invention disclosure based on the work presented in this paper.

[1]To whom correspondence may be addressed. Email: ssuresh@ntu.edu.sg or kjhsia@cmu.edu.

This article contains supporting information online at www.pnas.org/lookup/suppl/doi:10.1073/pnas.1717912115/-/DCSupplemental.

(25, 26). In this work, we observed continuous polymerization during growth of postgelation hydrogel, a process that better resembles tissue growth in nature. Such a growth mechanism relies on the continued diffusion of monomers into the porous hydrogel. We demonstrate that such continuous polymerization can be manipulated by controlling oxygen (O_2) concentration, where O_2 plays a role in polymerization similar to the role of growth factors in tissue growth. We further show that by controlling local chemistry, material structure, and mechanical constraints, the PA gel can self-assemble into complex biomimetic 3D morphologies. The current method provides a model system to study, among other phenomena, the mechanisms underlying the influence of light and gravity on the orientation of plant stem, the formation of saddle-shaped tree leaves and flowers via differential growth, and the evolution of wavy patterns in the airways of asthma patients. Since the continuous growth mode is a general principle for most living systems undergoing morphogenesis, our technique can be a powerful tool to study many growth phenomena in living systems. Appropriate adaptations of this method could point to pathways for generating complex 3D structures in applications as diverse as tissue engineering, soft robotics, and flexible electronics.

Oxygen Diffusion-Mediated Polymerization

Our approach relies on the premise that hydrogel gelation process can be modulated by controlling the distribution of polymerization inhibitors in gel solution. Specifically, polymerization is initiated by catalysts which turn initiators into free radicals (27, 28). These free radicals then activate monomers and cross-linkers into new free radicals that can further react with inactivated monomers and cross-linkers, resulting in cross-linked hydrogel network. Because the polymerization rate largely relies on the availability and abundance of free radicals in the reaction system, this process is susceptible to the existence of free-radical inhibitors, molecules that can convert free radicals into much less reactive or even nonreactive counterparts. O_2, as a common inhibitor, can turn free radicals into peroxyl radicals that have insufficient reactivity to continue polymer chain growth, and therefore slows down the gelation process (28). Polymerization could be even completely inhibited when dissolved O_2 reaches a critical concentration (29). Therefore, special treatments to minimize dissolved O_2 have often been performed in preparing hydrogel (30). In this work, we take advantage of the detrimental effect of O_2 on polymerization of PA hydrogel and turn it into an approach to manipulate the gelation process. The reaction scheme of PA hydrogel in our experiments is described in more detail in *Supporting Information*.

In our experiments, we intentionally allow the gel solution to polymerize under the open-air condition, instead of preventing the gel solution from being exposed to O_2. Under this condition, polymerization is a dynamic reaction–diffusion process as illustrated in Fig. 1*A*. The ambient air maintains a constant O_2 concentration ($c_0 = 20.9\%$ vol/vol) at the liquid–air interface. As dissolved O_2 is completely removed before introducing catalysts and initiators, the concentration gradient drives O_2 to continuously diffuse from the liquid–air interface into gel solution once the polymerization is initiated. This process leads to the termination of polymer chain growth by accumulated O_2 near the liquid–air interface. Visible gelation is then possible only in the region away from the interface. We modify the surface hydrophobicity of our polydimethylsiloxane (PDMS) reaction chamber (*Materials and Methods*) to demonstrate how O_2 concentration can be strategically controlled to produce the desired shape of the hydrogel. The meniscus profile of gel solution inside the reaction chamber can be predicted with the open source Surface Evolver-Fluid Interface Tool (SE-FIT) (31) and used to estimate the distribution of O_2 during polymerization (*Materials and Methods*). As shown in Fig. 1*B*, a hydrophobic surface of our PDMS reaction chamber (wetting angle $\theta = 107.5 \pm 1.7°$, Fig. S1) gives rise to O_2 depletion at the center of the bottom of the chamber, leading to the formation of a disk-shaped hydrogel (Fig. 1*C1*). Plasma treatment switches the PDMS surface from hydrophobic to hydrophilic ($\theta = 14.3 \pm 1.0°$, Fig. S1) and consequently changes the meniscus shape from convex to concave. A hydrophilic PDMS surface gives rise to O_2 depletion at the corner of the chamber, forming a ring-shaped hydrogel (Fig. 1

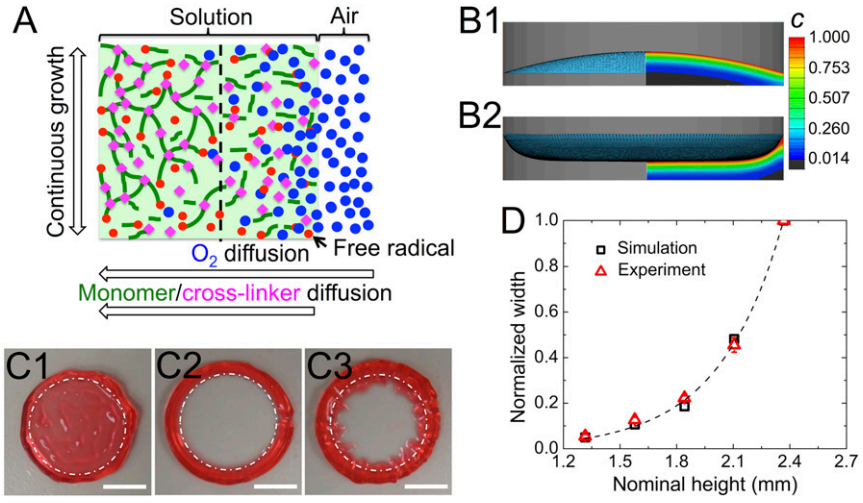

Fig. 1. Disk-to-ring transition of PA hydrogel via controlled oxygen diffusion with the modification of surface hydrophobicity. (*A*) Schematic representation of the polymerization process. Gelation occurs because of diffusion-mediated oxygen inhibition only on the left side of the black dashed line. (*B*) Simulated menisci of the gel solution inside a cylindrical PDMS chamber without (*B1*) and with (*B2*) plasma treatment, respectively, overlaid with contour plots of the oxygen concentration inside the gel solution after 265 s. Bulk liquid exists below the meniscus. Oxygen concentration is normalized by the concentration at the liquid–air interface. Gelation regions (black) are identified as the region where normalized oxygen concentration is below 1.4% (29). (*C*) Dimensions of polymerized hydrogel without (*C1*) and with (*C2* and *C3*) plasma treatment after taking the specimen out of the reaction chamber. The initial nominal liquid heights, the volume of the gel solution normalized by the bottom area of the chamber, are 1.84 mm for *C1* and *C2* and 2.10 mm for *C3*. White dashed circles indicate the size of the reaction chamber. (Scale bars: 1 cm.) (*D*) Experimental and simulation results of the normalized ring width, i.e., the width of the ring structure normalized by the radius of the chamber, as a function of the nominal height of the gel solution.

C2 and *C3*). Simple diffusion simulations of O_2 concentration (Fig. 1*B*) allow us to predict the disk-to-ring transition (Fig. 1*C*), and predict the increase of the ring-wall width with increasing initial volume of gel solution. The predicted ring-wall width agrees well with experimental results (Fig. 1*D*).

We also note that the polymerization of PA hydrogel proceeds in a unique growth mode benefiting from its porous structure. As shown in Fig. 1*A*, the copolymerization of monomers and cross-linkers in the gelation region (on the left of the dashed line) results in a concentration gradient of the free monomers and cross-linkers, from high concentration near the liquid–air interface to low concentration inside the cross-linked hydrogel. Benefiting from its porous nature, free monomers and cross-linkers are able to diffuse into the cross-linked hydrogel network from the liquid gel solution region. Meanwhile, as pointed out earlier, O_2 concentration is also low inside the hydrogel, thus facilitating continued polymerization in postgelation region. This unique growth mode is evidenced by the emergence of buckling of the hydrogel ring as its continued growth is confined by the reaction chamber (Fig. S2). Fig. 1*C* shows that upon taking polymerized hydrogel out of the reaction chamber, the radius of the hydrogel disk and that of the hydrogel ring are bigger than the reaction chamber dimension (the reaction chamber dimension is depicted by the white dashed-line circles). It is worth noting that this internal growth mode of hydrogel is fundamentally different from that of crystal growth during which new constituent atoms, molecules, or ions are added to the outer surface of an ordered crystal lattice (4, 32). In fact, this growth mode is more similar to living tissue growth through cell enlargement and division. During living tissue growth the growth factors dictate the synthesis of new biomass from available nutrients, whereas during hydrogel growth the O_2 concentration regulates the rate of gelation. The diffusion of monomers and cross-linkers, on the other hand, resembles the transport of nutrients.

Biomimetics of Tissue Morphogenesis

We further demonstrate the similarities between our method for continuous polymerization of hydrogel and several biological processes by successfully reproducing the complex shapes found during tissue morphogenesis in both plants and animals (Fig. 2).

i) The directional bending of plant stems responding to change of direction of gravity or sunlight is a good example of how the local chemistry (in this case, auxin) regulates tissue morphogenesis. In gravitropism, the sedimentation of statoliths, dense organelle in cells in the endodermic layer of the stem, activates the mechanosensitive signaling pathways which transport auxins to the lower part of the stem (33). Enhanced auxin concentration locally promotes stem growth. The differential growth between upper and lower parts of the stem therefore leads to upward bending of the stem (Fig. 2*A*). In our experiments of hydrogel polymerization, O_2 regulates the reaction rate, leading to the differential growth-induced directional bending of the hydrogel structure. As shown in Fig. 2*B*, a rectangular hydrogel ring formed in a rectangular chamber is regulated by an O_2 concentration gradient, from high concentration near the inner side (exposed to ambient air) to low concentration near the outer side (near the chamber wall). The polymerization rate therefore is higher near the outer side, resulting in a residual compressive strain on the outer side while a tensile strain develops on the inner side (Fig. 2*B*). As shown in our experimental results (Fig. 2*C*), when the mechanical constraint is relieved by slicing the hydrogel open, directional bending toward the inner side occurs. A similar observation with a circular hydrogel ring is shown in Fig. S3.

ii) Material heterogeneity within a single tissue serves as a catalyst for creating differential growth in living tissues. During such differential growth, the region that grows relatively more slowly imposes a mechanical constraint on the region where growth occurs faster. For example, the growth rate difference in a leaf between the slow-growing midvein and the fast-growing edge leads to the emergence of a saddle-shaped configuration (34), as shown in Fig. 2*D*. To mimic this phenomenon, we introduce a soft cotton wire along the long axis of an elliptical chamber (Fig. 2*E*). The geometric constraint imposed by the soft wire effectively suppresses the local hydrogel growth near the wire, whereas regions away from the wire undergo continuous internal growth. As shown in Fig. 2*F*, a saddle-shaped configuration is formed after the hydrogel is taken out of the reaction chamber.

iii) However, another example is the morphogenesis of human respiratory airways in asthma patients. Compared with normal airways, the airways in asthma patients undergo significant architectural remodeling, including swollen airway lining and tightened smooth-muscle constraint (35). As shown in Fig. 2*G*, the smooth muscles in the outermost layer of the airway impose a stiff geometric constraint to the swelling of the soft airway lining, causing constriction and an undulating pattern of the airway canal. In the hydrogel experiment, we regenerate a buckled wavy pattern on the inner wall by prescribing a stiff circular line constraint, similar to that of the stiff smooth-muscle layer in asthma patients (Fig. 2*H*).

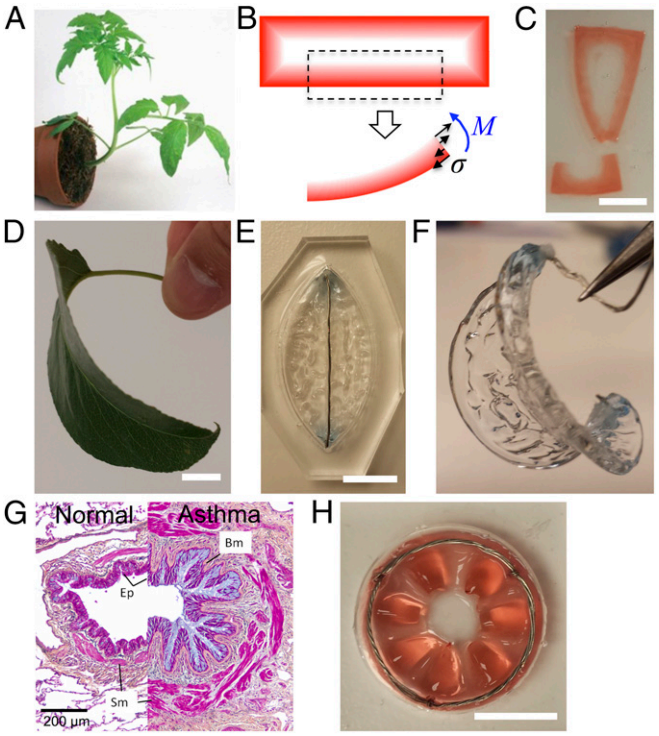

Fig. 2. Biomimetics of the morphogenesis of plant and animal tissues. (*A*) Directional bending of plant stem in gravitropism (image from internet). Schematic (*B*) and experimental (*C*) demonstrations of directional bending of a rectangular hydrogel ring through oxygen diffusion-mediated differential polymerization. (*D*) Representative image of saddle-shaped leaf. (*E* and *F*) Polymerized PA gel in an elliptical chamber with geometric constraint imposed by a soft wire before (*E*) and after (*F*) being taken out of the chamber. (*G*) Movat's pentachrome stain of human normal and asthmatic airways (35). (*H*) Polymerized hydrogel with circular line constraint. (Scale bars: 1 cm.)

Three-Dimensional Architecture Generation

Besides providing possible insights into morphogenesis of living tissues, the current method offers a means to generate complex

soft 3D architectures in hydrogels. Fig. 3 shows that by controlling polymerization and mechanical constraints, the hydrogel self-assembles into 3D bowls with and without ruffled edges. Differential growth is introduced by submerging a stiff circular wire in gel solution. While the presence of the wire suppresses local growth of the hydrogel, hydrogel continues to grow at the inner part of the disk and at the outer edge. Depending on the location of the constraining wire, the residual strain due to differential growth, upon releasing the hydrogel from the reaction chamber, gives rise to a bowl-shaped structure with either a flat edge (Fig. 3, top row), or a buckled, wavy edge (Fig. 3, bottom row). Through a combination of the bottom-up approach that controls O_2 diffusion-regulated polymerization, and the top-down approach that introduces mechanical constraints, we develop a powerful approach to generate complex 3D architectures, as demonstrated in Fig. S4.

We further demonstrate another strategy to generate complex 3D architectures facilitated by regional differential growth of hydrogel during polymerization. The bottom surface of our reaction chamber can be chemically activated to enhance its adhesion with hydrogel (*Materials and Methods*). Specifically, the activated regions feature a layer of aldehyde groups that can form covalent bonds with the free amine groups in PA hydrogel (36). The strong adhesion between hydrogel and chemically activated bottom surface effectively suppresses the internal growth of hydrogel (Fig. S5). As proof of concept, we selectively activate the bottom surface such that strong adhesion between hydrogel and bottom surface is possible only within specified regions (Fig. S6). As shown in Fig. 4, hydrogel forms covalent bonds with the bottom surface within branch patterns, serving as anchoring sites (blue regions in Fig. 4). The continuous growth in nonadhered regions leads to out-of-plane buckling, rendering 3D buckled hydrogel ring architectures. More complex 3D architectures can be readily generated following this strategy.

Discussion

In summary, we demonstrate an approach to generate complex hydrogel-based 3D architectures via controlled molecular self-assembly of monomers and cross-linkers. In general, complex 3D shapes in soft materials can be realized through two distinct approaches. The top-down approach involves engineering heterogeneous, patterned structures (layered, directionally stiffened or softened, residually stressed, etc.) which, upon stimulation or release of constraints, evolve into 3D shapes (17, 24, 37, 38). The bottom-up approach utilizes the material's ability to self-assemble

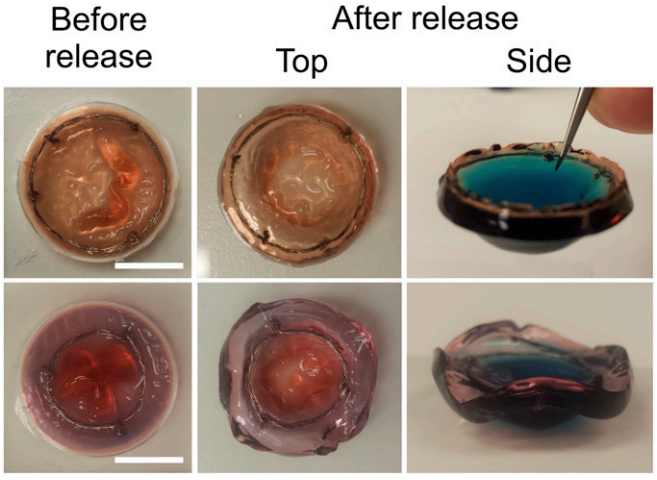

Fig. 3. Self-assembled 3D soft hydrogel bowls with and without a wavy edge. Blue food-dye solution is held in the bowls to demonstrate their structural integrity. (Scale bars: 1 cm.)

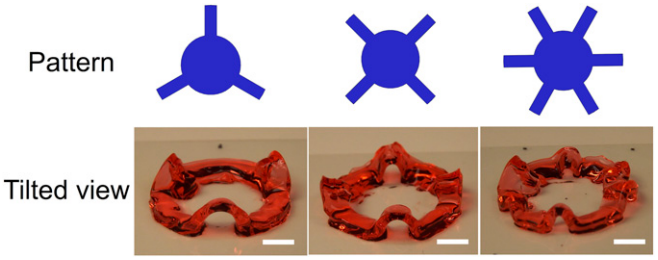

Fig. 4. Three-dimensional hydrogel architectures generated with selectively patterned glass substrates. Blue regions denote the activated regions that can chemically bind with PA hydrogel. (Scale bars: 1 cm.)

or grow into 3D shapes (e.g., tissues and organs of animals, and leaves and flowers of plants). Sometimes combined top-down/bottom-up approaches are needed to achieve special functions or shapes of a soft structure/device. The vast majority of techniques to date make use of the top-down approach. The current study thus demonstrates possibilities for generating 3D architectures in soft materials using a bottom-up method. Our approach relies on the porous nature of cross-linked network, so that continuous transport of monomers and cross-linkers into postgelation network is permitted, facilitating continuous growth of hydrogel. Differential growth of hydrogel can be effectively introduced when mechanical constraints are incorporated into the polymerization system. We demonstrate that this approach can serve as a powerful means to generate biomimetic and other complex soft 3D architectures. Because this unique growth mode is expected to be a general principle for all polymer materials that feature a porous structure after polymerization, our findings are likely to be applicable to a wide variety of fields, such as biomedical engineering, polymer science, soft robotics, and flexible electronics.

Materials and Methods

Meniscus Shape and O_2 Distribution Prediction. For a given volume of gel solution, we numerically predict the surface profile inside a cylindrical chamber using the open-source SE-FIT software. The prebuilt Z-cylindrical container is used with the contact angle measured experimentally. The equilibrium surface profiles obtained with a surface tension $\gamma = 0.072$ N/m and gravity acceleration $g = 9.8$ m/s^2 are exported from SE-FIT and reconstructed in the commercial software ABAQUS (39) to simulate the dynamics of oxygen diffusion. We model the O_2 diffusion as an equivalent axisymmetric thermal conduction problem. The diffusivity of oxygen inside the gel solution ($D = 8 \times 10^{-6}$ cm^2/s) (29) is converted to an equivalent thermal diffusivity. Oxygen diffusion from the PDMS side is negligible for the following reasons and therefore not considered in our simulations. First, the diffusivity of O_2 in PDMS is comparable to that in gel solution (40), but the thickness of the PDMS wall is one order of magnitude larger than the height of the gel solution. In addition, plasma treatment generates a silica layer on the PDMS surface which further limits the diffusion of O_2 significantly. The four-node axisymmetric convection/diffusion quadrilateral element is used for the simulation.

Contact Angle Measurement. The contact angle between gel solution and PDMS surface is measured using a ramé-hart Contact Angle Goniometer (ramé-hart instrument co.). The gel solution is a mixture of 10% acrylamide and 0.1% bis-acrylamide (AMRESCO) in deionized water. To prepare PDMS substrates, a 10:1 weight mixture of base to curing agent (Sylgard 184; Dow Corning) is thoroughly mixed, degassed, and cured at 65 °C for 2 h. During the measurement, small droplets of gel solution are placed onto flat PDMS substrates using a micropipette, while the built-in camera system simultaneously records the droplet profile from which the instant contact angle is automatically calculated in the DROPimage software (ramé-hart instrument co.). The volume of the gel solution droplet is gradually increased from 1 μL until the contact angle starts to decrease. The maximum equilibrium contact angle is used as the default contact angle between the gel solution and the PDMS substrate. Measurements are performed on both PDMS substrates with and without plasma treatment. Plasma treatment is performed for 1 min at a high power level (18 W) using a plasma cleaner (Harrick Plasma), and the same setting is used for all plasma treatments performed in this study.

Reaction Chamber Construction. A reaction chamber is an assembly of a PDMS ring on a glass coverslip. To prepare the mold for making the PDMS ring, circular patterns with a diameter of 22.2 mm are cut out of a 6.35-mm-thick acrylic sheet using a laser cutter (Epilog Laser) and then glued onto the bottom surface of a Petri dish using a two-part epoxy (Gorilla Epoxy; Gorilla Glue Inc.). PDMS rings are prepared using a 10:1 weight mixture of base to curing agent. After curing at 65 °C for 2 h, PDMS rings are carefully removed from the mold and assembled onto a glass coverslip with gentle pressure.

Glass Surface Activation. To activate the glass surface, coverslips are plasma-treated for 1 min, followed by 30 min incubation in 4% 3-aminopropyltrimethoxysilane (APTMS; Sigma-Aldrich) in isopropanol, and then 30 min incubation in 1% glutaraldehyde solution (Alfa Aesar). PDMS molds with various numbers of branch structures are used to confine the glass surface that exposes to the glutaraldehyde solution, yielding selectively functionalized patterns.

Polymerization. Before polymerization, the gel solution is degassed for at least 30 min in a vacuum desiccator to completely remove dissolved oxygen. Polymerization is then initiated by introducing tetramethylethylenediamine (TEMED; Teknova) and ammonium persulfate (APS; Promega) into the gel solution with final concentrations of 0.3% and 0.05%, respectively. The gel solution of a desired volume is immediately pipetted into the polymerization chamber with minimal disturbance so as to avoid introducing oxygen. The solution is allowed to react for 3 h before replacing the unpolymerized solution with food-dye solution to stain the polymerized hydrogel for imaging purpose. The reaction chamber is disassembled after the completion of polymerization to release hydrogel structures.

ACKNOWLEDGMENTS. Research reported in this publication was supported by Eunice Kennedy Shriver National Institute of Child Health and Human Development Grant R01HD086325. C.H., D.Q., and K.J.H. also acknowledge financial support from Carnegie Mellon University.

1. Hangarter RP (1997) Gravity, light and plant form. *Plant Cell Environ* 20:796–800.
2. Shyer AE, et al. (2013) Villification : How the gut gets its villi. *Science* 342:212–218.
3. Ward PS, Thompson CB (2012) Signaling in control of cell growth and metabolism. *Cold Spring Harb Perspect Biol* 4:a006783.
4. Kaplan CN, et al. (2017) Controlled growth and form of precipitating microsculptures. *Science* 355:1395–1399.
5. Nelson EC, et al. (2011) Epitaxial growth of three-dimensionally architectured optoelectronic devices. *Nat Mater* 10:676–681.
6. Meyer zu Heringdorf FJ, Reuter MC, Tromp RM (2001) Growth dynamics of pentacene thin films. *Nature* 412:517–520.
7. Baumgartner J, et al. (2013) Nucleation and growth of magnetite from solution. *Nat Mater* 12:310–314.
8. Bilsborough GD, et al. (2011) Model for the regulation of Arabidopsis thaliana leaf margin development. *Proc Natl Acad Sci USA* 108:3424–3429.
9. Benková E, et al. (2003) Local, efflux-dependent auxin gradients as a common module for plant organ formation. *Cell* 115:591–602.
10. Ingber DE (2005) Mechanical control of tissue growth: Function follows form. *Proc Natl Acad Sci USA* 102:11571–11572.
11. Pan Y, Heemskerk I, Ibar C, Shraiman BI, Irvine KD (2016) Differential growth triggers mechanical feedback that elevates Hippo signaling. *Proc Natl Acad Sci USA* 113: E6974–E6983.
12. Li B, Cao Y, Feng X, Gao H (2012) Mechanics of morphological instabilities and surface wrinkling in soft materials : A review. *Soft Matter* 8:5728–5745.
13. Liu Z, Swaddiwudhipong S, Hong W (2013) Soft matter pattern formation in plants via instability theory of hydrogels. *Soft Matter* 9:577–587.
14. Liang H, Mahadevan L (2011) Growth, geometry, and mechanics of a blooming lily. *Proc Natl Acad Sci USA* 108:5516–5521.
15. Tallinen T, Chung JY, Biggins JS, Mahadevan L (2014) Gyrification from constrained cortical expansion. *Proc Natl Acad Sci USA* 111:12667–12672.
16. Mora T, Boudaoud A (2006) Buckling of swelling gels. *Eur Phys J E Soft Matter* 20: 119–124.
17. Motala MJ, et al. (2015) Programming matter through strain. *Extreme Mech Lett* 3: 8–16.
18. Epstein E, Yoon J, Madhukar A, Hsia KJ, Braun PV (2015) Colloidal particles that rapidly change shape via elastic instabilities. *Small* 11:6051–6057.
19. Abdullah AM, Nan K, Rogers JA, Hsia KJ (2016) Mismatch strain programmed shape transformation of curved bilayer-flexible support assembly. *Extreme Mech Lett* 7: 34–41.
20. Klein Y, Efrati E, Sharon E (2007) Shaping of elastic sheets by prescription of non-Euclidean metrics. *Science* 315:1116–1120.
21. Kim J, Hanna JA, Byun M, Santangelo CD, Hayward RC (2012) Designing responsive buckled surfaces by halftone gel lithography. *Science* 335:1201–1205.
22. Abdullah AM, Braun PV, Hsia KJ (2016) Programmable shape transformation of elastic spherical domes. *Soft Matter* 12:6184–6195.
23. Lee H, Zhang J, Jiang H, Fang NX (2012) Prescribed pattern transformation in swelling gel tubes by elastic instability. *Phys Rev Lett* 108:214304.
24. Gladman AS, Matsumoto EA, Nuzzo RG, Mahadevan L, Lewis JA (2016) Biomimetic 4D printing. *Nat Mater* 15:413–418.
25. Drury JL, Mooney DJ (2003) Hydrogels for tissue engineering: Scaffold design variables and applications. *Biomaterials* 24:4337–4351.
26. Slaughter BV, Khurshid SS, Fisher OZ, Khademhosseini A, Peppas NA (2009) Hydrogels in regenerative medicine. *Adv Mater* 21:3307–3329.
27. Giz A, Çatalgil-Giz H, Alb A, Brousseau JL, Reed WF (2001) Kinetics and mechanisms of acrylamide polymerization from absolute, online monitoring of polymerization reaction. *Macromolecules* 34:1180–1191.
28. Decker C, Jenkins AD (1985) Kinetic approach of o2 inhibition in ultraviolet and laser-induced polymerizations. *Macromolecules* 18:1241–1244.
29. Hepworth SJ, Leach MO, Doran SJ (1999) Dynamics of polymerization in polyacrylamide gel (PAG) dosimeters: (II) modeling oxygen diffusion. *Phys Med Biol* 44:1875–1884.
30. Oytun F, Kahveci MU, Yagci Y (2013) Sugar overcomes oxygen inhibition in photoinitiated free radical polymerization. *J Polym Sci* 51:1685–1689.
31. Chen Y, Schaeffer BM, Weislogel MM (2011) Introducing SE-FIT: Surface Evolve-Fluid Interface Tool for studying capillary surfaces. *Proceedings 49th AIAA Aerospace Sciences Meeting Including the New Horizons Forum and Aerospace Exposition* (American Institute of Aeronautics and Astronautics, Orlando, FL), 2011–1319.
32. Noorduin WL, Grinthal A, Mahadevan L, Aizenberg J (2013) Rationally designed complex, hierarchical microarchitectures. *Science* 340:832–837.
33. Vanneste S, Friml J (2009) Auxin: A trigger for change in plant development. *Cell* 136: 1005–1016.
34. Liang H, Mahadevan L (2009) The shape of a long leaf. *Proc Natl Acad Sci USA* 106: 22049–22054.
35. Wadsworth SJ, Dorscheid DR, Yang SJ (2012) *IL-13, Asthma and Glycosylation in Airway Epithelial Repair* (INTECH Open Access Publisher, Rijeka, Croatia), pp 187–228.
36. Tse JR, Engler AJ (2010) Preparation of hydrogel substrates with tunable mechanical properties. *Curr Protoc Cell Biol* Chapter 10:Unit 10.16.
37. Zhang Y, et al. (2017) Printing, folding and assembly methods for forming 3D mesostructures in advanced materials. *Nat Rev Mater* 2:17019.
38. Chun IS, Challa A, Derickson B, Hsia KJ, Li X (2010) Geometry effect on the strain-induced self-rolling of semiconductor membranes. *Nano Lett* 10:3927–3932.
39. Dassault Systèmes (2014) ABAQUS Documentation (Dassault Systèmes, Providence, RI), Version 6.14.
40. Markov DA, Lillie EM, Garbett SP, McCawley LJ (2014) Variation in diffusion of gases through PDMS due to plasma surface treatment and storage conditions. *Biomed Microdevices* 16:91–96.